

Magnetic activity and accretion on FU Tau A: Clues from variability

Alexander Scholz^{1*}, Beate Stelzer², Grainne Costigan¹, David Barrado^{3,4},
Jochen Eisloffel⁵, Jorge Lillo-Box³, Pablo Riviere-Marichalar³, Hristo Stoev³

¹ School of Cosmic Physics, Dublin Institute for Advanced Studies, 31 Fitzwilliam Place, Dublin 2, Ireland

² INAF - Osservatorio Astronomico di Palermo, Piazza del Parlamento 1, I-90134 Palermo, Italy

³ Centro de Astrobiología Depto. Astrofísica (INTA-CSIC), ESAC campus, P.O. Box 78, E-28691 Villanueva de la Cãnada, Spain

⁴ Calar Alto Observatory, Centro Astronómico Hispano Alemán, Almería, Spain

⁵ Thüringer Landessternwarte Tautenburg, Sternwarte 5, D-07778 Tautenburg, Germany

Accepted. Received.

ABSTRACT

FU Tau A is a young very low mass object in the Taurus star forming region which was previously found to have strong X-ray emission and to be anomalously bright for its spectral type. In this study we discuss these characteristics using new information from quasi-simultaneous photometric and spectroscopic monitoring. From photometric time series obtained with the 2.2m telescope on Calar Alto we measure a period of ~ 4 d for FU Tau A, most likely the rotation period. The short-term variations over a few days are consistent with the rotational modulation of the flux by cool, magnetically induced spots. In contrast, the photometric variability on timescales of weeks and years can only be explained by the presence of hot spots, presumably caused by accretion. The hot spot properties are thus variable on timescales exceeding the rotation period, maybe due to long-term changes in the accretion rate or geometry. The new constraints from the analysis of the variability confirm that FU Tau A is affected by magnetically induced spots and excess luminosity from accretion. However, accretion is not sufficient to explain its anomalous position in the HR diagram. In addition, suppressed convection due to magnetic activity and/or an early evolutionary stage need to be invoked to fully account for the observed properties. These factors cause considerable problems in estimating the mass of FU Tau A and other objects in this mass/age regime, to the extent that it appears questionable if it is feasible to derive the Initial Mass Function for young low-mass stars and brown dwarfs.

Key words: stars: low-mass, brown dwarfs; stars: rotation; stars: activity; accretion, accretion discs

1 INTRODUCTION

FU Tau has been known for several decades as a variable star embedded in the dark cloud B215 (e.g. Gotz 1961; Romano 1975) and as a member of the Taurus star forming region based on H α emission and proper motion (Haro et al. 1953; Jones & Herbig 1979). Recently the object has drawn interest because it turned out to be a binary, with a primary component FU Tau A and the faint companion FU Tau B at a separation of 5.7", corresponding to a projected separation of ~ 800 AU for the distance of Taurus. Luhman et al. (2009) discovered the companion and estimated spectral types of M7.25 and M9.25 and masses of 0.05 and 0.015 M_{\odot}

for the two objects, indicating that FU Tau may in fact be a rare wide binary brown dwarf. Because of the wide separation of the two components and the location far away from any other member of the star forming region, FU Tau is of considerable interest to test formation scenarios for substellar objects.

Apart from its binarity and location, FU Tau A turns out to exhibit two other anomalous properties. First, the object has strong X-ray emission compared with other objects at similar spectral type (Stelzer et al. 2010). Moreover, the X-ray spectrum indicates the presence of soft radiation, possibly from an accretion-related shockfront, as has been observed previously for more massive objects (e.g. Stelzer & Schmitt 2004). Second, FU Tau A is anomalously bright for objects of this spectral type in the Taurus star

* E-mail: aleks@cp.dias.ie

forming region. It sits about one order of magnitude above the 1 Myr isochrone in the HR diagram (Luhman et al. 2009; Stelzer et al. 2010). In Stelzer et al. (2010) a few possible scenarios have been put forward to explain these features, including suppressed convection due to magnetic activity, excess flux from accretion, and early evolutionary stage.

Here we set out to put further constraints on the properties of FU Tau A by analysing its photometric and spectroscopic variability. This paper is mainly based on photometric time series obtained with the instruments CAFOS and BUSCA at the 2.2 m telescopes of the German-Spanish Astronomical Center at Calar Alto observatory. In Sect. 2 we discuss these observations and the reduction of the data. The analysis of the photometry and spectroscopy is presented in Sect. 3 and 4. In Sect. 5 we compile all available information on the variability of the system from our new observations, the literature, and archives and constrain the origin of the variations using spot models. We discuss the results in the context of the two anomalies mentioned above in the final Sect. 6.

2 OBSERVATIONS AND DATA REDUCTION

2.1 CAFOS

2.1.1 Imaging

Our primary photometric time series was obtained with CAFOS at the 2.2 m telescope on Calar Alto over five nights in Nov/Dec 2010. CAFOS is a $2 \times 2k$ CCD camera mounted in the RC focus. With a pixel scale of $0''.53$, it gives a field of view (FOV) of $16' \times 16'$. The filters, however, do not cover the full FOV; in effect a circular FOV with diameter of $\sim 14'$ can be used.

While the whole run was affected by dodgy weather conditions, including bad seeing, high humidity, and clouds, we obtained 62 useful images in the R-band and the same number in the I-band for our target. The final night of the run we observed Landolt standard stars under photometric conditions for calibraton purposes (2x field SA92, 3x field SA98). The observing log for the run is given in Table 1.

FU Tau is located in the middle of a dark cloud devoid of stars. Since we need non-variable field stars to calibrate the lightcurves, our FOV was not centered on FU Tau itself. Instead, we positioned FU Tau in the south-west (SW) corner of the CCD, which allows us to cover a sufficient number of field stars in the area immediately north-east (NE) of the cloud. To minimize flatfield problems, we aimed to keep the position of the time series field as constant as possible; the offsets between the images are $< 10''$. We also aimed to keep the flux level of FU Tau A roughly constant, i.e. we varied the exposure times to account for changes in seeing and transparency.

For all images we carried out a standard reduction: subtracting the average bias level and dividing by a scaled, averaged domeflat. We found that the flatfielding is not perfect; the resulting frames are affected by a large-scale interference pattern, which might be due to water condensation on the detector window. The effect increases with the time offset between science frames and domeflats. Therefore we obtained two sets of domeflats per night and corrected the images using the flatfield with the minimum time off-

Table 1. Time series observations with CAFOS and BUSCA. In the 2nd column, the 'C' stands for CAFOS and the 'B' for BUSCA. The values for exposure times and seeing are typical for a particular night.

Date	bands	no.	exp time	seeing
2010-11-28	C/R,I	6	250, 100	2''
2010-11-30	C/R,I	21	450, 120	3-4''
2010-12-01	C/R,I	8	300, 100	2''
2010-12-02	C/R,I	27	300, 80	2''
2010-12-08	B/I	2	120	2''1
2010-12-10	B/I	5	120	1''7
2010-12-11	B/I	6	120	1''6
2010-12-13	B/I	1	120	1''5
2010-12-15	B/I	4	120	2''4

set. Since the pattern has a spatial scale of $> 50''$ and the spatial offsets in the time series are $< 10''$ we do not think that the pattern has an effect on the lightcurves. In addition, the I-band frames show a faint small-scale interference pattern due to nightsky emission lines, which contributes to the noise.

2.1.2 Spectroscopy

As part of the same run, we obtained 5 low-resolution spectra for FU Tau A, using grism R400 with a nominal resolution of 10 \AA .

The spectra for FU Tau A were debiased and background-subtracted by fitting a 2nd order polynomial to each line in the spatial direction. They were extracted, dispersion-corrected and flux-calibrated using standard routines in IRAF.

2.2 BUSCA

Complementary time series photometry in the I-band was obtained using BUSCA at the 2.2 m telescope on Calar Alto. BUSCA allows to take images in four bands simultaneously, achieved through 3 dichroic beam splitters. Our target, however, was not detected in the three blue channels (Stromgren vby filters); we only use the images in the reddest channel, which corresponds to the Cousins I-band. The observations started about a week after the CAFOS run and continued for another week. Similar to the CAFOS run, parts of the observations were affected by clouds, strong winds, and high humidity. No photometric calibration was carried out.

An $11' \times 11'$ FOV centered on FU Tau was observed in 7 nights in Dec 2010, of which 5 provided usable data (see Table 1). The FOV covers the bright K2III star 2MASS J04232455+2500084 and 5-10 point sources 1-2 mag fainter than FU Tau A. For all images, we carried out a standard reduction including bias subtraction and flatfield correction.

3 TIME SERIES PHOTOMETRY

3.1 Photometry and relative calibration

From the CAFOS time series we derived R- and I-band lightcurves for FU Tau A. We hand-picked a sample of 48

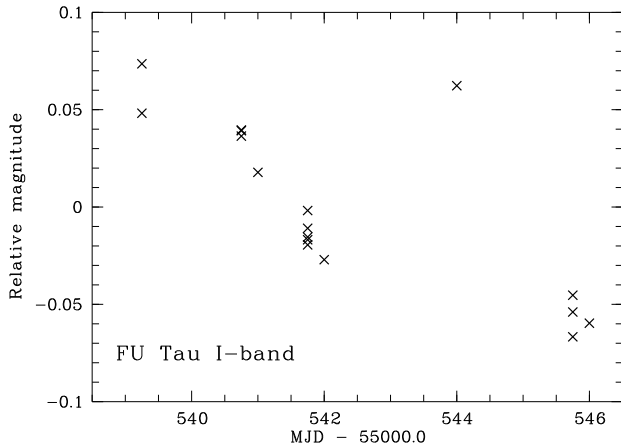


Figure 2. I-band lightcurve for FU Tau A derived from the BUSCA images.

(I) and 45 (R) sources, including FU Tau A and all other isolated stars with similar brightness in the FOV. For these objects we carried out aperture photometry using a constant aperture of 10 pixel and a sky annulus of 10-20 pixel. Due to the poor seeing, the companion FU Tau B is not detected in most of the CAFOS images; no photometry was possible for this object.

To correct for the effects of variable seeing and transparency (‘relative calibration’), we calculated the average time series of non-variable stars in the field and subtracted it from all lightcurves. The non-variable stars were chosen using the procedure outlined in Scholz & Eisloffel (2004). The routine selected 18 (R) and 10 (I) stars as non-variable, based on a comparison of their lightcurve with the average lightcurve of all other stars. The average RMS of the lightcurves for these non-variable stars is 0.010 (R) and 0.012 mag (I), which defines the photometric accuracy.

From the BUSCA images we obtained I-band lightcurves for FU Tau A and all other stars in the field, again using aperture photometry with the same parameters as for CAFOS. The bright star 2MASS J04232455+2500084 clearly looks variable, but 7 faint field stars show stable lightcurves. Their average lightcurve is used for the relative calibration. After subtraction of the average lightcurve, the RMS for the 7 field stars is 0.011-0.025, an average of 0.018 mag, confirming that they are non-variable. For comparison, the RMS for 2MASS J04232455+2500084 is 0.13 mag.

3.2 Lightcurve analysis

The lightcurves from CAFOS and BUSCA show that FU Tau A is a variable star. Its RMS is 0.04 (R-band, CAFOS), 0.02 (CAFOS, I-band), and 0.04 (BUSCA, I-band), significantly more than comparison stars (0.01 mag for CAFOS, 0.02 mag for BUSCA, Sect. 3.1). The lightcurves from CAFOS and BUSCA are shown in Figs. 1 and 2. Most of the variability is on timescales of > 1 d; these variations are intrinsic to the source and are not seen in the reference stars.

In addition, the CAFOS lightcurves show intra-night variability with smaller amplitude. These variations, however, are partly seen in the reference stars as well. FU Tau

A is by far the reddest object in our sample. The influence of the atmospheric conditions is colour-dependent, which is not taken into account in our correction. Thus, one could expect the reddest objects to show some residuals of the trends caused by atmospheric effects. Hence, we do not consider the low-level intra-night variability in FU Tau A to be real.

Using all available CAFOS datapoints for a given filter, we searched for a period using a combination of three routines. The R- and the I-band lightcurves show a dominant peak in the CLEANed periodogram (Roberts et al. 1987) at a period of 3.8 (R) and 4.0 d (I). The same peak is detected in the Scargle periodogram (Scargle 1982) with a false alarm probability below 10^{-5} (calculated following Horne & Baliunas (1986)). In the Scargle periodogram, however, the peak is very broad and does not permit an accurate assessment of the period. Finally, we compare the RMS in the original lightcurve with the RMS after subtracting a sine function with the suspected period using the F-test. Again, the period of 3.7-4.0 d is highly significant in both bands, with false alarm probabilities below 10^{-5} . In Fig. 3 we show the phase-folded lightcurve assuming $P = 3.8$ d, which we consider to be the best-fitting period from all three algorithms. The observing run covers only one period, and the sampling of the period is patchy (in phase space). Therefore, a relatively large range of periods (3.5-4.1 d) give a decent fit to the data, i.e. the uncertainty in the period is in the range of ± 0.3 d.

Although the coverage with BUSCA is not sufficient to carry out an independent period search, we use these datapoints to check the period derived from the CAFOS lightcurves. In Fig. 4 we show a phaseplot for all I-band data, assuming a period of 3.8 d (left panel) and 4.2 d (right panel). A good match is achieved for a period of 4.2 d, slightly larger than the period determined from the R- and I-band CAFOS lightcurves. A period of 3.8 d only matches if a significant phase shift between the CAFOS and the BUSCA data is assumed.

3.3 Calibrated photometry

From the Landolt standard fields observed in the last night of the CAFOS run we derived a photometric calibration. In total, we observed 45 standards from which 40 gave useful photometry. These stars cover a wide range in airmass from $X = 1.3$ to 2.0. For the R-band the absolute magnitudes R are well reproduced with a zeropoint shift and an extinction term: $R = r - 1.647 - 0.147X$. The RMS for this transformation is 0.03, dominated by the uncertainty in the zeroterm. For the I-band, it turns out that an additional colour term improves the RMS from 0.1 to 0.05: $I = i - 2.281 - 0.069X + 0.136(r - i)$. (In these equations, the lower case letters are instrumental magnitudes and upper case letters calibrated magnitudes.)

Applying this transformation to the instrumental magnitudes measured for FU Tau A gives $R = 15.39$ and $I = 13.73$ mag for the night 2010-12-02. For this night the lightcurve for FU Tau A indicates a photometric uncertainty of ~ 0.02 mag (see Sect. 3.2). Adding this in quadrature to the calibration errors, the total uncertainty in the absolute magnitudes is 0.04 in the R-band and 0.05 in the I-band.

Published photometry in similar bands for FU Tau A is

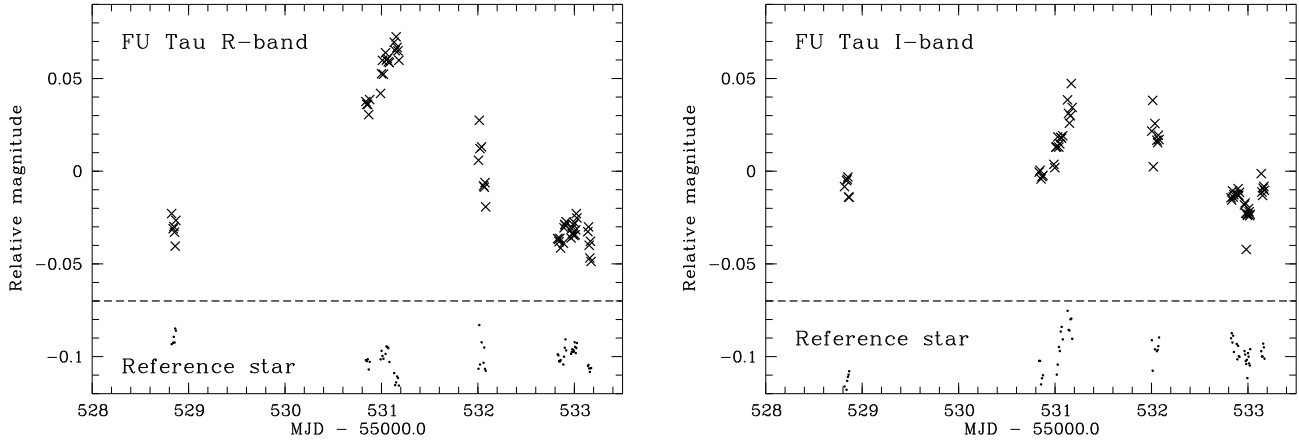


Figure 1. Lightcurves for FU Tau A derived from the CAFOS images for the R- and the I-band. In addition to the target, we show the lightcurve of a similarly bright, non-variable reference star in the same field. The intra-night variability of FU Tau A is partly seen in the reference stars as well and could be due to secondary extinction effects and not intrinsic to the source. The inter-night variability, however, is not apparent in the reference stars.

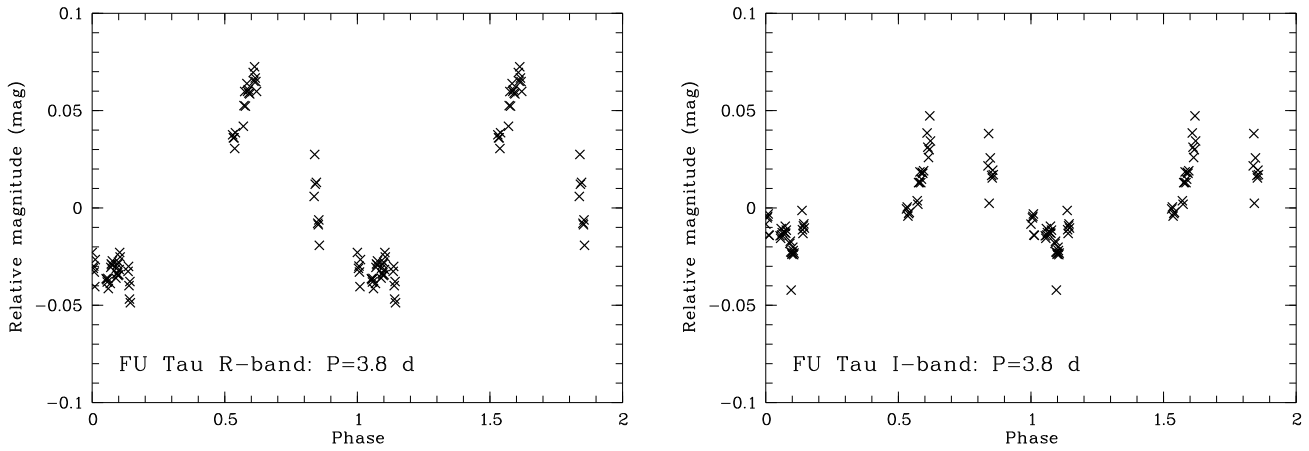


Figure 3. Phase-folded lightcurves for FU Tau A assuming our best-fitting period of 3.8 d, determined from the CLEANed periodograms. The typical error is 0.010 mag in R and 0.012 mag in I.

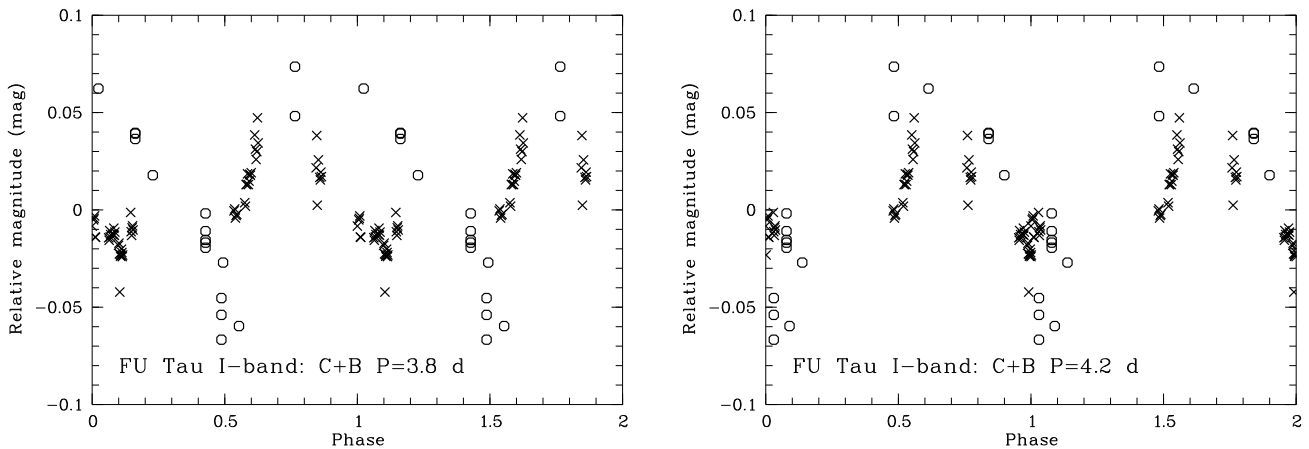


Figure 4. Phase-folded I-band lightcurves for FU Tau A showing the datapoints from CAFOS (crosses) and BUSCA (circles) for two different periods. The typical error is 0.012 mag for CAFOS and 0.018 mag for BUSCA.

Table 2. Calibrated photometry for FU Tau A in bands similar to Johnson R and I. Typical errors are 0.05 mag.

Date	Sloan r	Sloan i	John R	John I	Comment
Oct 2001	16.94				CMC14 ¹
06/12/2002	17.13	14.86	16.41	13.92	Sloan ^{2,3}
29/12/2002 ⁴	16.86	14.75	16.18	13.85	Sloan ^{2,3}
29/12/2002				13.58	CFHT ²
02/12/2010			15.39	13.73	CAFOS ⁵

¹ Evans et al. (2002)

² Luhman et al. (2009)

³ Sloan magnitudes converted to Johnson using equations in Jordi et al. (2006)

⁴ Conflicting epoch information in Luhman et al. (2009) (29 or 31/12/2002)

⁵ this paper

available from CFHT (Cousins I), Sloan (r, i), and the Carlsberg Meridian Catalog 14 (filter close to Sloan r). To transform the Sloan magnitudes to the Johnson/Cousins system, we used Equ. (2) and (8) from Jordi et al. (2006). All calibrated photometry in the bands R and I is listed in Table 2. The band transformations from Sloan to Cousins depend linearly on $R - I$ and are only calibrated for $0 < R - I < 2$, whereas FU Tau A is slightly redder ($R - I = 2.3 - 2.5$) in the Sloan photometry. There is, however, no evidence for additional colour trends for $R - I < 2$ in Fig. 3 of Jordi et al. (2006), i.e. any error introduced by this conversion is likely to be small.

The two epochs of Sloan photometry differ by 0.07 in I and 0.23 in R over a timescale of 23-25 d, which is slightly more than our amplitudes measured over 5 nights. Comparing our photometry with the Sloan values indicates long-term variability of 0.2 mag in I and 0.9 mag in R . FU Tau A was much fainter and also redder in $R - I$ in 2002 compared with 2010 ($R - I \sim 2.4$ vs. 1.7 mag).

The Sloan and CFHT photometry has been measured in December 2002. In Luhman et al. (2009) the epochs are listed as Dec 6 and 29 in their Table 1 and as Dec 6 and 31 in the text. FU Tau is not listed in the 6th data release of the Sloan Digital Sky Survey (Adelman-McCarthy & et al. 2008) referenced by Luhman et al. (2009), and not in the 7th data release either, therefore we cannot verify the exact source of the photometry. According to Luhman et al. (2009) the CFHT data is from Dec 29.

The I-band difference between the second Sloan epoch and CFHT of 0.27 mag seems quite a lot compared with the low level of variability in our lightcurve (≤ 0.05 mag in one night, 0.09 mag over 4 nights, Sect. 3.2). The large difference could be due to a) inconsistencies in the I-band calibration, b) problems with the transformation from Sloan to Cousins bands (see above), or c) a strong outburst in that particular night. For these reasons we cannot reliably use the CFHT I-band magnitude and disregard the datapoint in the following. The CMC14 datapoint was obtained in October 2001 and is consistent with the Sloan r-band value from December 2002.

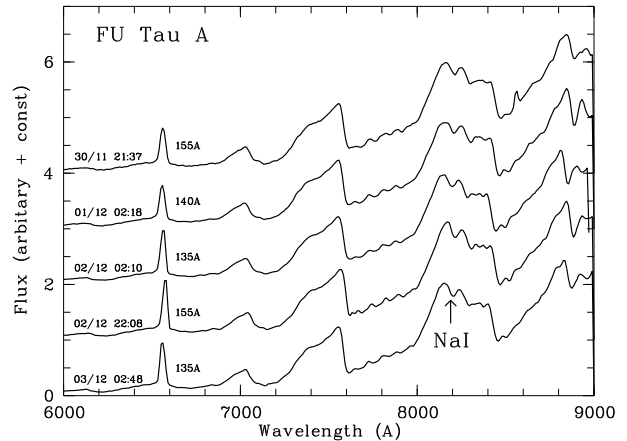


Figure 5. Low-resolution spectroscopy for FU Tau A from CAFOS. The dates and times of the observations and the equivalent widths for $H\alpha$ are indicated. The NaI absorption feature is marked. The resolution is 10 \AA .

4 SPECTROSCOPY

The five CAFOS spectra for FU Tau A, obtained in 4 different nights in Nov/Dec 2010, are shown in Fig. 5. The spectral shape is remarkably similar; we do not find any significant differences in the continuum. With our low resolution of 10 \AA , the $H\alpha$ feature at 6563 \AA is the only emission feature. The equivalent widths (EW) for this line are in the range of $135\text{--}155 \text{ \AA}$ and are indicated in Fig. 5. The variations in the EW are not significantly larger than the uncertainty, which is in the range of $\pm 10\text{--}20 \text{ \AA}$. The EWs are also consistent with the value of 146 \AA measured from a Gemini/GMOS spectrum in March 2008 (Stelzer et al. 2010).

Using the PC3 index suggested by Martín et al. (1999) we assigned spectral types. In chronological order, the spectral types are M6.82, M6.86, M6.67, M6.72, M6.66, i.e. the change is only ± 0.1 subtypes. Compared with the uncertainties, this is not a significant variation. Thus, the photometric variability observed for FU Tau A does not manifest itself as a change in spectral type. This is not particularly surprising, as the colour variation in $R - I$ over this time series is only 3% (Table 3).

The $H\alpha$ EW of FU Tau A is well-above the usually adopted threshold between non-accreting 'weak-line' and accreting 'classical' T Tauri stars (CTTS). According to Barrado y Navascués & Martín (2003), all M7 objects with $H\alpha$ EW $> 40 \text{ \AA}$ should be considered to be accretors. FU Tau A's status as substellar analog to a CTTS is confirmed by the presence of mid-infrared excess (Luhman et al. 2009), most likely from a circumstellar disk, and a wealth of other accretion-related emission lines in the optical and near-infrared spectrum (Stelzer et al., in prep.).

The spectra also clearly show the NaI absorption features at $\sim 8200 \text{ \AA}$, which is in fact a doublet of lines at 8183 and 8195 \AA (Kirkpatrick et al. 1991). The feature is sensitive to surface gravity and can be used as an age indicator for cool stars. In our spectra the EW for NaI are $3\text{--}3.5 \text{ \AA}$. For comparison, objects with similar spectral type as FU Tau A have typical NaI EW of $6\text{--}8 \text{ \AA}$ in the field, $5\text{--}6 \text{ \AA}$ in the 100 Myr old cluster Pleiades, and $1.5\text{--}3.5$ in the 3 Myr old

Table 3. Photometric amplitudes for FU Tau A as a function of filter and timescale

Filter	λ (μm)	Δt	A (mag)
Johnson I	0.85	4 d	0.09 ± 0.02^1
Johnson R	0.65	4 d	0.12 ± 0.02^1
Johnson I	0.85	7 d	0.14 ± 0.03^1
Sloan z	0.89	23 d	0.07 ± 0.07^2
Sloan i	0.75	23 d	$0.09 \pm 0.07^{2,3}$
Sloan r	0.62	23 d	$0.27 \pm 0.07^{2,4}$
Sloan g	0.47	23 d	0.44 ± 0.07^2
Sloan u	0.36	23 d	0.71 ± 0.08^2
Johnson I	0.85	8 yr	$0.2 \pm 0.1^{1,2}$
Johnson R	0.65	8 yr	$0.9 \pm 0.1^{1,2}$
IRAC2	4.5	2 yr	0.19 ± 0.03^2
IRAC4	8.0	2 yr	0.25 ± 0.04^2

¹ this paper² Luhman et al. (2009)³ translates to Johnson I amplitude of 0.07⁴ translates to Johnson R amplitude of 0.23

σ Ori cluster (Steele & Jameson 1995; Kenyon et al. 2005). Thus, our NaI measurement confirms the youth of FU Tau A.

5 ORIGIN OF THE VARIABILITY

The available photometry for FU Tau A provides an account of its variability on timescales ranging from hours to years. While our photometric time series with CAFOS and BUSCA covers the short-term variations (a week or less) in the optical, the archived data in the literature from Sloan and Spitzer constrains the long-term changes in the optical and infrared. In Table 3 we compile the variability amplitudes for FU Tau A from a variety of sources. In the following we aim to use the characteristics of this dataset to constrain the physical properties of FU Tau A, in particular the presence of cool spots caused by magnetic activity and/or hot spots caused by the accretion flow.

As demonstrated in this paper, FU Tau A shows small-scale variations of ~ 0.1 mag in the I- and R-band on timescales of a few days, with a periodicity in the range of 4 d (Sect. 3.2). A plausible explanation for this behaviour is the presence of asymmetrically distributed surface spots which cause a modulation of the observed flux due to the rotation of the object, a behaviour typical for many young low-mass stars (Herbst et al. 2007). The amplitudes are slightly larger in the R-band by factor of 1.3, as expected for cool spots (Bouvier et al. 1995).

Simple spot simulations were used to constrain the properties of the spots. We calculate the flux ratio between the spotless surface of FU Tau and the surface with a single spot with a certain temperature T_S and filling factor f (defined as the fraction of the surface covered by the spot). For the spectrum of the unspotted photosphere, we used the AMES-DUSTY spectrum (Allard et al. 2001) for $T = 3000$ K and $\log g = 3.5$, typical of very young objects. Note that the actual temperature of the unspotted photosphere is not known. Based on the average spectral type of

M6.75 (Sect. 4), we would estimate 2800 K (Mentuch et al. 2008), but if spots are present the unspotted photosphere will be hotter. We ran the same simulations for $T = 2800$ and 3200 K. Since this gives only marginally different results, the exact choice of T does not seem to be relevant.

The spot spectrum was approximated either by the AMES-DUSTY spectrum or with a blackbody. We calculated flux ratios as a function of wavelength for T_S ranging from 1500 to 4000 K in steps of 100 K and f ranging from 0.01 to 0.3 in steps of 0.01. For the blackbody spot, we extended the temperature range to 4500 K.

To compare these ratios with the observations, we calculated the amplitudes m_R and m_I for the wavelengths of the respective filters and derived the following test quantity:

$$\chi^2 = \frac{1}{N} \sum_{i=1}^N \frac{(\Delta X - m_X)^2}{\delta X^2} \quad (1)$$

Here ΔX are the observed amplitudes, δX their errors (both from Table 3), m_X the amplitudes from the simulations and N is the number of filters. A good fit will result in $\chi^2 < 1$.

In Fig. 6, upper row, we show the results for the CAFOS data; all parameter combinations with $\chi^2 < 1$ are plotted with crosses, the ones with $\chi^2 < 3$ with dots. In both types of simulations, the observed amplitudes are best-matched by cool spots with $f \sim 0.1$. Not surprisingly, the match is better when the spot is modeled with the AMES-DUSTY spectrum, as cool spots are expected to have a spectrum resembling a cool photosphere. Hot spots, on the other hand, do not provide a good match. This result becomes stronger when we consider that the CAFOS amplitudes are likely to be somewhat smaller, as the lightcurves are affected by atmospheric effects (Sect. 3.2).

The variations on timescales of 1-3 weeks are constrained by the BUSCA lightcurve and the Sloan photometry. Here the amplitudes tend to be somewhat larger than on the 4 d timescale covered by CAFOS. Moreover, the amplitude ratio between the R- and I-band in the Sloan data is a factor of 3 larger than in the CAFOS lightcurves. The Sloan photometry indicates a steep increase of the amplitudes towards shorter wavelengths, which is typical for hot spots, as already discussed in Stelzer et al. (2010). We ran the same spot simulations as before for the Sloan amplitudes (2nd section in Table 3) and plot the results in Fig. 6 (lower left panel). This time only hot spots with $f < 0.1$ provide a decent match. Not shown are the results for spots with AMES-DUSTY spectrum, because this series of simulations does not give any match with $\chi^2 < 3$.

The best way to constrain the long-term optical variations on timescales of years is the comparison between our dataset and Sloan in the R- and I-band (3rd section in Table 3). Here the R-band amplitude is by a factor of 4.5 larger than the I-band amplitude. Again, the simulations essentially rule out cool spots, but give a good match for a variety of parameter combinations for hot spots (Fig. 6, lower right panel). As this test is based only on two bands, the results do not provide particularly good constraints on the spot parameters. The simulation for the two Sloan epochs (see above) with five filters, including the blue bands, probably gives a better idea of the hot spot properties.

We also explored the possibility of having hot and cool spots simultaneously on the surface of FU Tau A. Using

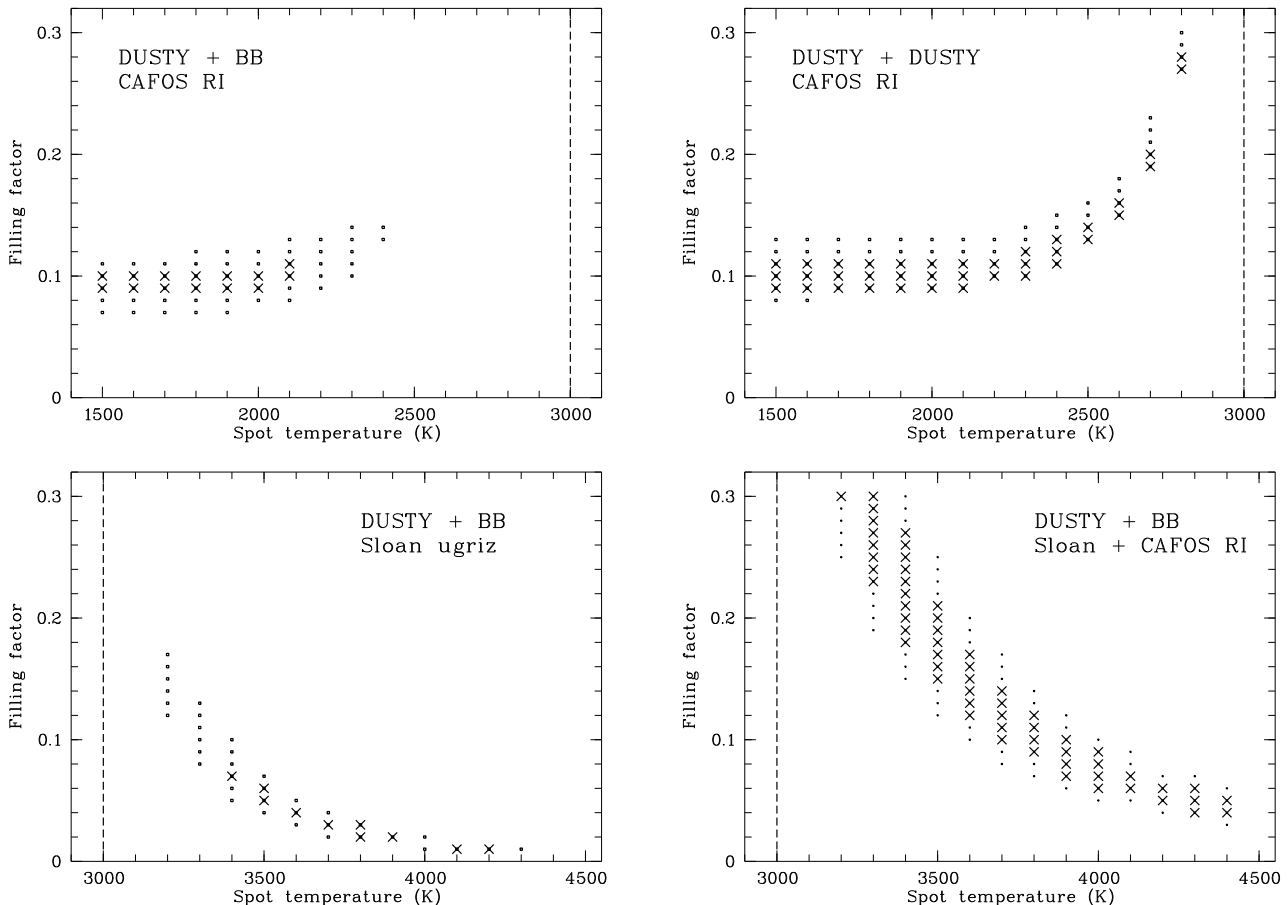


Figure 6. Best-fitting spot temperature/filling factor combinations from the simulations discussed in Sect. 5. All crosses show the best fitting combinations with $\chi^2 < 1$, all dots with $\chi^2 < 3$.

the Sloan amplitudes in five bands and adopting a filling factor of 5% (for hot and cool spots, respectively) yields a good match with $\chi^2 < 1$ for $T_{\text{hot}} = 3500 - 3600$ K and $T_{\text{cool}} = 2000 - 2900$ K. For higher filling factors, T_{hot} decreases, and vice versa. Thus, the combination of hot and cool spots definitely fits the observed amplitudes.

We conclude that the periodic modulation on a timescale of 4 d is best explained by cool spots co-rotating with the object. On longer timescales of weeks to years, however, the optical variability is dominated by hot spots. The cool spots are asymmetrically distributed and thus cause a periodic, rotational signal. The hot spots, on the other hand, are axisymmetric (e.g., limited to the polar regions) and stable in size/location over timescales of at least 4 d, but vary on longer timescales.

The cool spots are most likely caused by suppressed convection due to magnetic field lines penetrating through the photosphere, as commonly observed for magnetically active stars, including the Sun. The hot spots could be indicative of the same phenomenon: If most of the surface is covered by cool spots, the few remaining areas of unspotted photosphere would be observed as hot spots. This would, however, require implausibly large filling factors of $> 70\%$, because the hot spot solutions in the simulations give filling factors below 30%.

The more probable option is that the hot spots are

shock fronts caused by gas accretion from the disk onto the object. This is also supported by the presence of H α emission in the spectra, which is likely to be dominated by accretion as well (Sect. 4). The lack of variability in H α over timescales of 4 d (EW varies by $< 10 - 15\%$) is in line with the presence of stable accretion-related spots. If accretion is the origin of the hot spots, the long-term variability in FU Tau A indicates substantial changes in the accretion configuration (geometry or accretion rate) on timescales of years.

In addition to the optical variability, FU Tau also exhibits moderate changes of ~ 0.2 mag at wavelengths of 3-8 μm on timescales of years (4th section in Table 3), which are significantly larger than the photometric error. The best explanation for the infrared variations is changes in the disk structure or temperature, which could be related to changes in the accretion flow.

6 DISCUSSION: THE NATURE OF FU TAU A

FU Tau A is anomalous in its observed properties, primarily in two aspects:

1) In comparison with Taurus objects of similar spectral type and temperature, FU Tau A shows strong X-ray emission, although still consistent with the large scatter (see Fig. 3 in Stelzer et al. 2010). Moreover, the X-ray emission

is dominated by a soft radiation component, which may be explained by emission from an accretion shock.

2) FU Tau A is overluminous in the HR diagram, with respect to the other known brown dwarfs of Taurus and to the theoretical 1 Myr isochrone (see Fig. 4 in Stelzer et al. 2010). This has been shown based on a luminosity calculated from the J-band magnitude ($L_{\text{bol}}/L_{\odot} = 0.2$, Luhman et al. 2009). We re-determined the luminosity by comparing model spectra with the full set of optical and near-infrared photometry (SDSS ugriz, 2MASS JHKs) using VOSA (Bayo et al. 2008), and find $L_{\text{bol}}/L_{\odot} = 0.19 \dots 0.21$, confirming the literature value.

Since the overluminosity of FU Tau A is central for the following arguments, we verify this claim by plotting FU Tau A and B in a magnitude vs. effective temperature diagram together with other late-type members of Taurus. As a comparison sample, we use the census by Rebull et al. (2010), which comprises spectroscopically confirmed members of Taurus. Their sample of previously known members contains 215 objects, out of which 186 have a spectral type in the literature and 2MASS photometry. We limit ourselves to objects with spectral type later or equal M4, $A_V < 5$ mag. Since FU Tau A and B are a Class II source based on their SED and have low extinction (Luhman et al. 2009), we also exclude sources with the SED type 'Class I' or 'flat' and with $A_V > 5$ mag. This leaves 71 objects out of which 35 have a disk according to the Spitzer data and 20 are detected in X-rays according to XEST¹ (Güdel et al. 2007).

For these objects we determined A_V from the $J - K$ colour:

$$A_V = [(J - K) - (J - K)_0]/0.1844 \quad (2)$$

This is based on the extinction law by Cardelli et al. (1989) for $R_V = 4.0$. We use $(J - K)_0 = 1$ which is appropriate for this spectral type range, as outlined in Scholz et al. (2009). After correcting the J-band magnitudes for extinction, we subtracted a distance modulus of 5.73 mag for $d = 140$ pc, to yield the absolute J-band brightness M_J . Spectral types were converted to effective temperatures using the relation by Mentuch et al. (2008). For FU Tau A and the companion B we carried out the same procedure. For FU Tau A we adopted a spectral type of M7, the average of our result (Sect. 4) and the type given by Luhman et al. (2009). Since no J-band magnitude is available for FU Tau B, we started with its K-band magnitude (Luhman et al. 2010) and added 1.3 mag, which is the typical extinction corrected $J - K$ colour for Taurus members at spectral type \sim M9 or later. The resulting brightness-temperature diagram is shown in Fig. 7.

Our goal was to minimise systematic effects that could influence a comparison between FU Tau A and the other objects. The x-axis is affected by inconsistencies in spectral typing, which we estimate to be in the range of ± 0.5 subtypes, as most of the objects have been classified using similar procedures and in the optical wavelength regime. On the y-axis, we estimate an uncertainty of ± 0.3 mag which mostly comes from the extinction estimate. One problem could be additional flux from disks in the K-band, which would cause us to overestimate extinction and brightness of objects with

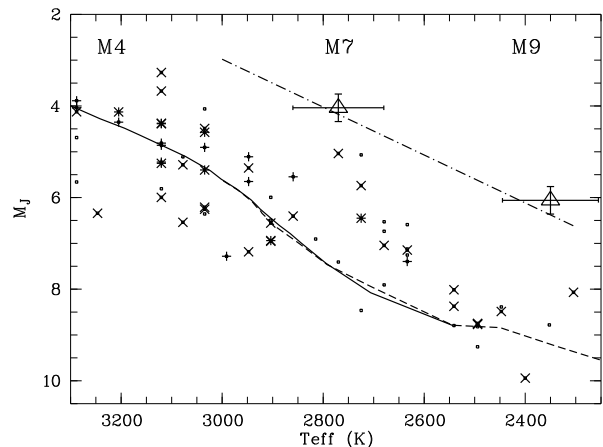


Figure 7. Absolute J-band magnitude vs. effective temperatures for FU Tau A and B (triangles) and other confirmed members of Taurus (dots, see text for selection criteria). Objects with disks are marked with crosses, those with X-ray detection with pluses. We overplot the BCAH (solid lines) and DUSTY (dashed lines) isochrone for an age of 1 Myr (Baraffe et al. 1998; Allard et al. 2001). The dashdotted line is a linear fit to the DUSTY isochrone shifted to match the positions of FU Tau A and B.

disks. In Fig. 7, however, no systematic difference is seen between objects with disks and those without, indicating that this effect is negligible.

Fig. 7 clearly demonstrates that FU Tau A is significantly brighter than all other similar objects in the Taurus star forming region with the same spectral type. The difference is ~ 1 mag compared with the brightest other objects at this spectral type or ~ 2 mag compared with the average brightness at this spectral type. As can be seen in the figure, the same offset is observed for FU Tau B, i.e. it cannot be explained by an effect that would only apply to FU Tau A, for example, an undetected close companion. One could explain the offset by lowering the distance of FU Tau to 90 pc or less, but this would place it outside the Taurus star forming region which makes it difficult to explain the young age of the system. In summary, the overluminosity of FU Tau A as well as the overluminosity of its companion is confirmed by our analysis.

In Stelzer et al. (2010) we suggest three plausible interpretations to explain the 2 anomalies discussed above: suppressed convection, accretion, and the evolutionary stage of the object. In the following we discuss these scenarios in light of the new analysis presented in this paper.

6.1 Suppressed convection

Strong magnetic activity could suppress the convection on the stellar surface and produce cool spots, as it seems to be the case in the primary of the eclipsing brown dwarf binary 2MASS J05352184-0546085 (Stassun et al. 2007). This would make FU Tau A appear cooler than it should be according to its mass, i.e. it would in fact be a very low mass star and not a brown dwarf. Correcting for this effect would shift FU Tau A roughly horizontally in the HR diagram towards higher temperatures and closer to the bulk of datapoints in Fig. 7. The same explanation could theoretically apply to FU Tau B.

¹ XMM-Newton Extended Survey of the Taurus molecular clouds

A higher mass would also help to explain the high X-ray luminosity (Stelzer et al. 2010), because of the well-known correlation between L_X and L_{bol} (e.g. Telleschi et al. 2007). In Fig. 7 we mark all objects with X-ray detection with plusses. The fraction of X-ray detected objects is only 2/29 (7%) for $T_{\text{eff}} < 2800$ K. In this temperature regime, FU Tau A is clearly an exception. For higher temperatures (2800-3300 K), the rate is 18/42 (42%) and the X-ray luminosity of FU Tau A would not be anomalous. In contrast to FU Tau A, the companion B is not detected in X-rays (Stelzer et al. 2010), which fits well into the lack of X-ray detections for objects below 2800 K.

The scenario of suppressed convection would require fast rotation, strong magnetic fields and/or magnetic spot coverage (Chabrier et al. 2007; MacDonald & Mullan 2009). The only way to definitely confirm it would be a model-independent mass estimate, which is not available for FU Tau A.

Indirectly, however, the new data supports the idea of suppressed convection. The presence of cool, magnetic spots is confirmed by the lightcurve analysis (Sect. 5), although the lightcurves can only detect asymmetrically distributed spots and cannot be used to fully characterise the spot distribution on the stellar surface. The rotation period of 4 d is quite long when compared with typical periods for young brown dwarfs (< 2 d, Scholz & Eislöffel 2005), but fits much better with the typical range of periods for young very low mass stars (2-5 d, Herbst et al. 2001). Thus, suppressed convection remains a plausible option.

6.2 Accretion

Accretion from a circumstellar disk might cause excess luminosity in the optical and near-infrared and shift objects vertically in Fig. 7. As said above, accretion might also be the best explanation for the soft X-ray emission in FU Tau A. Accretion is clearly ongoing, as evidenced by the optical spectra (this paper, Stelzer et al. in prep.). The long-term variability in FU Tau A can only be explained by excess flux from hot spots and could indicate variable accretion (Sect. 5). However, since the spot temperatures are not particularly high (< 5000 K) accretion is unlikely to cause a drastic over-estimate in the luminosity. For plausible spot parameters of $T_S = 4000$ K and $f = 0.1$ (see Fig. 6) the excess flux at $1.0 \mu\text{m}$ would only be in the range of 30%. It needs to be stressed, however, that the variability is caused only by the changes in the hot spots, i.e. higher excess luminosity from constant, axisymmetrically distributed spots is possible.

The interpretation of the high luminosity in terms of accretion would imply that the actual L_{bol} is much lower, leading to an unusually high fractional X-ray luminosity. If the luminosity is in fact one order of magnitude lower than given by Luhman et al. (2009), we would get $\log(L_X/L_{\text{bol}}) = -2.2$ (Stelzer et al. 2010), much more than the median for Taurus brown dwarfs (-4.0, Grosso et al. 2007), which would thus create a new anomaly. Also, some other very low mass objects in Taurus share the unusual characteristics of FU Tau A (position in Fig. 7 above the isochrone and strong X-ray emission), albeit not as extreme as our target, and some of them are not accreting. For these reasons, accretion is unlikely to be the only reason for the anomalies of FU Tau A.

Similar to FU Tau A, the companion FU Tau B shows strong $\text{H}\alpha$ emission and mid-infrared excess indicative of the presence of a disk (Luhman et al. 2009). Thus, accretion could also affect its position in Fig. 7.

6.3 Evolutionary stage

The overluminosity of FU Tau A and B could also be caused by extreme youth. If accretion occurs mostly in bursts ('episodic accretion'), objects which are technically 'coeval', i.e. have started their protostellar collapse at the same time, could be in a different stage of their accretion history and spread out in the HR diagram (Baraffe et al. 2009). Overluminous objects would be younger in terms of their accretion evolution.

In Fig. 7 we overplot the BCAH and DUSTY 1 Myr isochrones (Baraffe et al. 1998; Allard et al. 2001). The comparison with the Taurus members shows that most of them fall within ± 1 mag of this isochrone, indicating an average age of 1 Myr. The dash-dotted line is a linear fit to the DUSTY isochrones, shifted by 3 mag towards brighter absolute magnitudes. The locations of FU Tau A and B are well-approximated by this line, i.e. the two objects sit about 3 mag above the isochrone. The Baraffe et al. models do not include the formation process and accretion history (Baraffe et al. 2002), i.e. the comparison with the observations is limited. It does show, however, that FU Tau A and B have roughly equal distance from the isochrone on the y-axis, i.e. in terms of these models they can be considered to be coeval.

If extreme youth is the reason for the unusual brightness of the two FU Tau components, it seems surprising that no other typical signs of the earliest evolutionary stages of T Tauri stars are seen. The objects have low extinction and their SEDs are classified as Class II, i.e. they are not embedded in a thick protostellar envelope. Also, the current accretion rate of FU Tau A is relatively low and comparable to the other Class II objects of similar spectral type in Taurus ($10^{-9} - 10^{-10} M_{\odot} \text{yr}^{-1}$, Stelzer et al. 2010). In addition, Class 0/I protostars appear to show lower or similar X-ray luminosities than Class II sources (Prisinzano et al. 2008), e.g. extreme youth cannot explain the strong X-ray emission of FU Tau A. Thus, an early evolutionary stage is not an entirely satisfactory explanation.

6.4 Conclusions

In summary, FU Tau A is affected by accretion plus magnetic activity and possibly evolutionary stage as well. Although the observed properties of FU Tau A are anomalous, these three factors are not limited to this particular object. All young populations show substantial spread in the HR diagram and in the other relevant properties (e.g., X-ray luminosities, $\text{H}\alpha$ luminosities, rotation periods). Evidence for accretion and strong magnetic activity is commonly seen in classical T Tauri stars and brown dwarfs. FU Tau A (and its companion FU Tau B) happens to be a case which sticks out in some of its observed properties, but there is no reason to believe that it is unusual in its physical characteristics.

This could have important consequences for our understanding of the Initial Mass Function in the low-mass regime.

Even with the wealth of photometric and spectroscopic data available for FU Tau A, it is still not possible to estimate its mass reliably. Depending on the relative magnitude of the effects of suppressed convection and accretion, the mass could be anywhere between 0.05 and $0.2 M_{\odot}$, a factor of 4 uncertainty. In addition, the unknown evolutionary stage and accretion history means that we cannot trust the isochrones for mass estimates. Thus, barring a more complete understanding of magnetic activity and its effect on the observable properties as well as protostellar evolution it does not seem feasible to derive a mass function for very young very low mass stars and brown dwarfs.

ACKNOWLEDGMENTS

We thank the anonymous referee for a constructive report that helped to improve the paper. This publication is based on observations collected at the Centro Astronómico Hispano Alemán (CAHA) at Calar Alto, operated jointly by the Max-Planck Institut für Astronomie and the Instituto de Astrofísica de Andalucía (CSIC). Part of this work was funded by the Science Foundation Ireland through grant no. 10/RFP/AST2780 to AS, and the Spanish grants AyA2010-21161-C02-02, CSD2006-00070, PRICIT-S2009/ESP-1496. In this paper we make use of VOSA, developed under the Spanish Virtual Observatory project supported from the Spanish MICINN through grant AyA2008-02156.

NOTE ADDED IN PROOF

Regarding the discussion in Sect. 3.3, it was brought to our attention that the SDSS photometry for FU Tau A and B was published in the data release of the 'Low Galactic Latitude Fields', which are not part of the standard SDSS data releases (Finkbeiner et al. 2004). The correct epoch for the SDSS datapoints for FU Tau is Dec 31 (Luhman, private communication).

REFERENCES

- Adelman-McCarthy J. K., et al. 2008, *ApJS*, 175, 297
 Allard F., Hauschildt P. H., Alexander D. R., Tamanai A., Schweitzer A., 2001, *ApJ*, 556, 357
 Baraffe I., Chabrier G., Allard F., Hauschildt P. H., 1998, *A&A*, 337, 403
 Baraffe I., Chabrier G., Allard F., Hauschildt P. H., 2002, *A&A*, 382, 563
 Baraffe I., Chabrier G., Gallardo J., 2009, *ApJ*, 702, L27
 Barrado y Navascués D., Martín E. L., 2003, *AJ*, 126, 2997
 Bayo A., Rodrigo C., Barrado Y Navascués D., Solano E., Gutiérrez R., Morales-Calderón M., Allard F., 2008, *A&A*, 492, 277
 Bouvier J., Covino E., Kovo O., Martin E. L., Matthews J. M., Terranegra L., Beck S. C., 1995, *A&A*, 299, 89
 Cardelli J. A., Clayton G. C., Mathis J. S., 1989, *ApJ*, 345, 245
 Chabrier G., Gallardo J., Baraffe I., 2007, *A&A*, 472, L17
 Evans D. W., Irwin M. J., Helmer L., 2002, *A&A*, 395, 347
 Finkbeiner D. P., Padmanabhan N., Schlegel D. J., Carr M. A., Gunn J. E., Rockosi C. M., Sekiguchi M., et al. 2004, *AJ*, 128, 2577
 Gotz W., 1961, *Veroeffentlichungen der Sternwarte Sonneberg*, 5, 87
 Grosso N., Briggs K. R., Güdel M., Guieu S., Franciosini E., Palla F., Dougados C., Monin J.-L., Ménard F., Bouvier J., Audard M., Telleschi A., 2007, *A&A*, 468, 391
 Güdel M., Briggs K. R., Arzner K., Audard M., Bouvier J., Feigelson E. D., Franciosini E., Glauser A., Grosso N., Micela G., Monin J.-L., et al. 2007, *A&A*, 468, 353
 Haro G., Iriarte B., Chavira E., 1953, *Boletín de los Observatorios Tonantzintla y Tacubaya*, 1, 3
 Herbst W., Bailer-Jones C. A. L., Mundt R., 2001, *ApJ*, 554, L197
 Herbst W., Eislöffel J., Mundt R., Scholz A., 2007, *Protostars and Planets V*, pp 297–311
 Horne J. H., Baliunas S. L., 1986, *ApJ*, 302, 757
 Jones B. F., Herbig G. H., 1979, *AJ*, 84, 1872
 Jordi K., Grebel E. K., Ammon K., 2006, *A&A*, 460, 339
 Kenyon M. J., Jeffries R. D., Naylor T., Oliveira J. M., Maxted P. F. L., 2005, *MNRAS*, 356, 89
 Kirkpatrick J. D., Henry T. J., McCarthy Jr. D. W., 1991, *ApJS*, 77, 417
 Luhman K. L., Mamajek E. E., Allen P. R., Muench A. A., Finkbeiner D. P., 2009, *ApJ*, 691, 1265
 Luhman K. L., Mamajek E. E., Allen P. R., Muench A. A., Finkbeiner D. P., 2010, *ApJ*, 720, 1781
 MacDonald J., Mullan D. J., 2009, *ApJ*, 700, 387
 Martín E. L., Delfosse X., Basri G., Goldman B., Forveille T., Zapatero Osorio M. R., 1999, *AJ*, 118, 2466
 Mentuch E., Brandeker A., van Kerkwijk M. H., Jayawardhana R., Hauschildt P. H., 2008, *ApJ*, 689, 1127
 Prisinzano L., Micela G., Flaccomio E., Stauffer J. R., Megeath T., Rebull L., Robberto M., Smith K., Feigelson E. D., Grosso N., Wolk S., 2008, *ApJ*, 677, 401
 Rebull L. M., Padgett D. L., McCabe C.-E., et al. 2010, *ApJS*, 186, 259
 Roberts D. H., Lehar J., Dreher J. W., 1987, *AJ*, 93, 968
 Romano G., 1975, *Mem. Soc. Astron. Ital.*, 46, 81
 Scargle J. D., 1982, *ApJ*, 263, 835
 Scholz A., Eislöffel J., 2004, *A&A*, 419, 249
 Scholz A., Eislöffel J., 2005, *A&A*, 429, 1007
 Scholz A., Geers V., Jayawardhana R., Fissel L., Lee E., Lafreniere D., Tamura M., 2009, *ApJ*, 702, 805
 Stassun K. G., Mathieu R. D., Valenti J. A., 2007, *ApJ*, 664, 1154
 Steele I. A., Jameson R. F., 1995, *MNRAS*, 272, 630
 Stelzer B., Schmitt J. H. M. M., 2004, *A&A*, 418, 687
 Stelzer B., Scholz A., Argiroffi C., Micela G., 2010, *MNRAS*, 408, 1095
 Telleschi A., Güdel M., Briggs K. R., Audard M., Palla F., 2007, *A&A*, 468, 425